Flexible Control of Motor Units: Is the Multidimensionality of Motor Unit Manifolds a Sufficient Condition?

François DERNONCOURT[1], Simon AVRILLON[1,2], Tijn LOGTENS[1],
Thomas CATTAGNI[3], Dario FARINA[2] and François HUG[1,4]*

[1] Université Côte d'Azur, LAMHESS, Nice, France
[2] Department of Bioengineering, Faculty of Engineering, Imperial College London, London, United Kingdom
[3] Nantes Université, Laboratory "Movement, Interactions, Performance" (UR 4334), Nantes, France
[4] The University of Queensland, School of Biomedical Sciences, Brisbane, QLD, Australia

* Corresponding author
Prof. François Hug (https://orcid.org/0000-0002-6432-558X)
Université Côte d'Azur, LAMHESS, Nice, France
Francois.hug@univ-cotedazur.fr

Abbreviated title: Control and dimensionality of motor unit manifolds

Supplemental data availability: The entire dataset (raw and processed data) and codes are publicly available at:
https://figshare.com/s/45cecab12ec45658ef83
https://github.com/FrancoisDernoncourt/Motor_unit_flexibility

Conflict of interests: The authors declare no competing financial interests.

Funding resources: This study was funded by a grant from the French National Research Agency (ANR-24-CE17-5805; Neuromotor project). François Hug is supported by the French government, through the UCAJEDI Investments in the Future project managed by the ANR with the reference number ANR-15-IDEX-01. Dario Farina is supported by the European Research Council Synergy Grant NaturalBionicS (contract #810346), the EPSRC Transformative Healthcare, NISNEM Technology (EP/T020970), and the BBSRC, "Neural Commands for Fast Movements in the Primate Motor System" (NU-003743). The authors are grateful to the Université Côte d'Azur's Center for High-Performance Computing (OPAL infrastructure) for providing resources and support.

Author Contributions: Contribution and design of the experiment: FD, SA, FH; Collection of data: FD; Analysis and interpretation: FD, SA, TL, TC, DF, FH; Drafting the article or revising it for important intellectual content: FD, SA, TL, TC, DF, FH; All authors approved the final version of the manuscript.

Acknowledgements: We thank Vincent Malejac (Université Jean-Monnet) for his assistance with data collection.

Abstract

Understanding flexibility in the neural control of movement requires identifying the distribution of common inputs to the motor units. In this study, we identified large samples of motor units from two lower limb muscles: the vastus lateralis (VL; up to 60 motor units/participant) and the gastrocnemius medialis (GM; up to 67 motor units/participant). First, we applied a linear dimensionality reduction method to assess the dimensionality of the manifolds underlying the motor unit activity. We subsequently investigated the flexibility in motor unit control under two conditions: sinusoidal contractions with torque feedback, and online control with visual feedback on motor unit firing rates. Overall, we found that the activity of GM motor units was effectively captured by a single latent factor defining a unidimensional manifold, whereas the VL motor units were better represented by three latent factors defining a multidimensional manifold. Despite this difference in dimensionality, the recruitment of motor units in the two muscles exhibited similarly low levels of flexibility. Using a spiking network model, we tested the hypothesis that dimensionality derived from factorization does not solely represent descending cortical commands but is also influenced by spinal circuitry. We demonstrated that a heterogeneous distribution of inputs to motor units, or specific configurations of recurrent inhibitory circuits, could produce a multidimensional manifold. This study clarifies an important debated issue, demonstrating that while motor unit firings of a non-compartmentalised muscle can lie in a multidimensional manifold, the central nervous system may still have limited capacity for flexible control of these units.

Keywords: motor neuron, synergy, factor analysis, muscle, electromyography

Key points.

- To generate movement, the central nervous system distributes both excitatory and inhibitory inputs to the motor units.
- The level of flexibility in the neural control of these motor units remains a topic of debate with significant implications for identifying the smallest unit of movement control.
- By combining experimental data and in silico models, we demonstrated that the activity of a large sample of motor units from a single muscle can be represented by a multidimensional linear manifold; however, these units show very limited flexibility in their recruitment.

- The dimensionality of the linear manifold may not directly reflect the dimensionality of descending inputs but could instead relate to the organisation of local spinal circuits.

1. Introduction

To generate movement, the central nervous system distributes excitatory and inhibitory inputs to the spinal motor neurons. Observations of correlated or synchronized activity among motor units have led to the assumption that a substantial portion of the net excitatory input is shared across different motor units from the same pool (1–3). The combination of common inputs with the size principle (4) theoretically imposes rigid control on motor units, which is characterized by a consistent size-ordered recruitment pattern. Although this control strategy is computationally efficient at simplifying the neural control of motor units, it has been challenged by the concept of a more flexible control, in which motor unit recruitment may deviate from the size principle (5–9). Understanding the flexibility in motor unit recruitment requires the identification of the distribution of common inputs (10, 11).

One approach for identifying the structure of common inputs to motor units is to apply linear dimensionality reduction methods to a series of firing times for many units. This approach can capture common patterns in the firing activities of motor units within low-dimensional manifolds shaped by the dynamics of latent factors. Using this approach, the firing patterns of the motor units of certain muscles have been projected onto multidimensional manifolds (12–14). Such a multidimensional manifold of motor unit firings can be interpreted as the presence of multiple common inputs (11). This observation may align with the concept of task-dependent behaviour of motor units, and thus it may support flexibility in motor unit control, possibly of cortical origin (8). Although this interpretation is plausible, the neural pathways responsible for increasing the dimensionality of motor unit manifolds remain unclear. Motor neurons receive numerous excitatory and inhibitory inputs from both cortical and subcortical sources. As such, a multidimensional manifold could emerge from a single common input of a cortical origin combined with additional common inputs from subcortical sources. This interplay between inputs from different origins could explain the contradictory results among studies. For example, Bracklein et al. (15) observed that participants could not independently control the motor units of the tibialis anterior muscle, whereas Ricotta et al. (14) showed that the motor unit firings in this muscle lie in a multi-dimensional linear manifold.

In the present study, we hypothesized that common cortical projections to motor neurons are not necessarily the sole inputs that determine the dimensionality of the motor unit manifolds. Other types of inputs, not under direct cortical control, may also shape manifold's dimensionality. For example, the activity of Renshaw cells, which are activated by recurrent

collaterals of homonymous and heteronymous motor neurons (16, 17), can contribute to decorrelating motor unit activity (18). Therefore, this circuit can contribute to increasing the dimensionality of the firing manifold, without increasing the flexibility of volitional motor unit control. We assume that the flexible control of motor units is primarily determined by the number of cortical inputs, rather than by the total number of inputs shaping the dimensionality of the manifold. It is possible that, in some muscles, a multidimensional linear manifold underlies a single cortical input, resulting in a rigid control of motor units.

To test this hypothesis, we recorded large samples of motor units to unravel the low-dimensional structures of their inputs. We selected two lower limb muscles based on previous studies reporting different levels of correlated activity of their motor units, with the vastus lateralis (VL) exhibiting less correlated activity (19) compared to the gastrocnemius medialis (GM) (20). We investigated whether the expected difference in manifold dimensionality between the two muscles reflected different levels of flexibility in their motor unit activity, and therefore, different neural constraints on motor unit control. First, we assessed the dimensionality of the manifolds underlying motor unit activity during torque-matched isometric contractions. We then investigated the flexibility in motor unit control under two conditions: sinusoidal contractions with torque feedback and online control with visual feedback on motor unit firing rates. Despite the differences in linear manifold dimensionality between the muscles, both exhibited similar and very limited flexibility in motor unit control. Finally, we developed a simulation model that demonstrated that the multidimensionality of the linear manifold in the VL was compatible with the presence of a heterogeneous distribution of inputs to motor units, or specific configurations of recurrent inhibitory circuits, even with a single descending command. These results suggest that the VL motor units receive common inputs from various sources, not all of which are under volitional control. This study clarifies an important debated issue in motor unit control, by showing that motor unit firings can lie in a multidimensional manifold; however, it may still be impossible for the central nervous system to flexibly control these motor units.

2. Methods

2.1. Participants and ethical approval

The first experiment involved a series of isometric torque-matched knee extension and plantarflexion tasks. Nine physically active males (age: 26.7±7.6 years, height: 179.7±7.9 cm, body mass: 76.6±11.6 kg) performed the knee extension tasks while seven active males (age: 29.2±7.2 years, height: 176.8±2.8 cm, body mass: 77.8±10.1 kg) performed the plantarflexion tasks. Two participants performed both the knee extension and plantarflexion tasks in two separate sessions. Owing to the low number of identified motor units (typically fewer than 10), two participants were excluded from the analysis of the knee extension task, and one participant was excluded from the plantarflexion task.

The second experiment involved isometric knee extension or plantarflexion tasks, during which the participants controlled the activity of pairs of motor units using online visual feedback on their firing rate. Six physically active males performed the knee extension tasks (age: 29.2±7.9 years, height: 175.2 ±3.1 cm, body mass: 73.8±8.6 kg) and the plantarflexion tasks (age: 29.4±7.7 years, height: 176.2±3.9 cm, body mass: 74.8±8.4 kg). Five of these participants completed both tasks across two separate sessions.

Participants had no history of lower leg pain with limited function that required time off work or physical activity, or a consultation with a health practitioner in the previous 6 months. The procedures were approved by the ethics committee (CPP Ouest III; 23.00453.000166), and conducted in accordance with the Declaration of Helsinki, except for registration in a database. The participants were fully informed of any risks or discomfort associated with the procedures before providing written informed consent.

2.2. Experimental design

For the knee extension tasks, the participants sat on a dynamometer (S2P Ltd, Ljubljana, Slovenia, EN 60204-1) with their hips and right leg each flexed at 80° (0° being the neutral position). For the plantarflexion tasks, the participants sat on a dynamometer (Biodex System 3 Pro, Biodex Medical, USA) with their hips flexed at 80° and their right legs fully extended. The foot was placed perpendicular to the shank. During both tasks, inextensible straps were tightened to immobilize the torso, pelvis, and thighs on the test side. These isometric tasks were used in the two experiments. In the first experiment, the participants matched the visual torque feedback. In the second experiment, they aimed to modulate the activity of two motor units using online visual feedback displaying their firing rates. In both experiments, sessions

began with a standardized warm up, followed by three maximal voluntary contractions (MVC) for 3 s, with 60 s of rest in between. Peak MVC torque was considered as the maximal value obtained from a moving average window of 250 ms.

2.2.1. Experiment 1 (torque-matched contractions)

Participants performed four trapezoid isometric contractions, each consisting of a 5-s linear ramp-up, a 20-s plateau at 20% MVC, and a 5-s linear ramp-down, with 30-s of rest in between. Participants then performed sinusoidal contractions, producing torque oscillations at frequencies of either 0.25 Hz, 1 Hz, and 3 Hz. Each sinusoidal contraction consisted of a 5-s linear ramp-up to 20% MVC, followed by a 10-s plateau at 20% MVC, and 20 s of sinusoidal oscillations between 15% and 25% MVC. Each sinusoidal contraction was performed three times, with at least 60 s of rest in between. The order of the frequency conditions was intentionally not randomized to allow the participants to progressively familiarize themselves with faster oscillations. For the 3 Hz sinusoidal condition, auditory feedback was provided in addition to visual feedback using a metronome.

2.2.2. Experiment 2 (volitional control of motor units)

Participants performed a trapezoid isometric contraction consisting of a 5-s linear ramp-up, a 20-s plateau at either 10% (knee extension) or 20% MVC (plantarflexion), and a 5-s linear ramp-down (referred to as 'baseline' contraction). The lower torque level for the knee extension tasks was chosen to minimize fatigue, which develops faster during knee extension than plantarflexion (21). This baseline contraction was used to identify motor unit separation vectors (filters) offline, which were then reapplied in real-time to display the motor unit firing rate as a visual feedback (22). After a 15-30 min rest period during which automatic offline decomposition of the electromyographic (EMG) signals and manual editing of the motor units were performed, the participants performed four 20-s submaximal isometric contractions, with 1-min of rest in between. Only the torque feedback was provided to the participants during these contractions (referred to as "reference" contractions).

The rest of the experimental session consisted of a series of 10-s isometric contractions during which the participants were instructed to dissociate the activity of two motor units while maintaining constant knee extension (10% MVC) or plantarflexion (20% MVC) torque constant. Specifically, the activity of the two motor units was depicted in 2D space, where the *x*- and *y*- axes represented the firing rates of motor units #1 and #2, respectively. The scale of

each axis ranged from 0 to twice the average firing rate of the corresponding motor units measured during baseline contraction. This scaling ensured that the cursor was not biased towards any of the axes. Two target triangles were added to the 2D space, each with one corner on the coordinate origin and two sides as one axis (*x* or *y*), and a line forming an angle of 30° along this axis. In addition, real-time feedback on torque output was provided to the participants *via* a vertical gauge, which they were required to maintain within two lines representing ±5% of the target torque.

For a given pair of motor units, the participants performed two sets of ten 10-s contractions, with 10 s of rest between each contraction. The participants aimed to reach Targets 2 and 1 during the first and second sets, respectively. To move the cursor towards these targets, the participants were required to differentially alter the firing rates of the two motor units (i.e., an increase in one unit with no change or a decrease in the other unit). This procedure was repeated with two to four different pairs of motor units, depending on the participant. Each pair comprised a motor unit from each of two EMG grids (proximal and distal; see below), providing participants with information regarding the location of the motor units they were asked to control independently.

2.3. Decoding of motor unit firing activity

2.3.1. High-density surface electromyographic recordings

EMG signals were recorded from either the GM (plantarflexion) or the VL, RF, and VM (knee extension). For the first experiment, four adhesive grids of 64 electrodes (total of 256 electrodes) were placed over the VL (inter-electrode distance: 8 mm; GR08MM1305, OT Bioelettronica, Italy) or GM (inter-electrode distance: 4 mm; GR04MM1305, OT Bioelettronica, Italy). One grid each of 64 electrodes was placed over the RF and VM muscles (inter-electrode distance: 8 mm; GR08MM1305, OT Bioelettronica, Italy). For the second experiment, two adhesive grids of 64 electrodes (a total of 128 electrodes) were placed over the proximal and distal region of the VL (inter-electrode distance: 8 mm; GR08MM1305, OT Bioelettronica, Italy) or GM muscle (inter-electrode distance: 4 mm; GR04MM1305, OT Bioelettronica, Italy). Overall, this setup was selected to maximize the number of decomposed motor units (23).

Prior to electrode application, the skin was shaved and cleaned with an abrasive paste (Nuprep, Weaver and Company, USA). Adhesive grids were held on the skin using bi-adhesive foam layers (SpesMedica, Battipaglia, Italy). The skin-electrode contact was made

by filling the cavities of the adhesive layers with conductive paste (SpesMedica, Battipaglia, Italy). A reference electrode (5×5 cm; Kendall Medi-Trace; Covidien, Ireland) was placed over the right patella (knee extension tasks) or right tibia (ankle plantarflexion tasks), and a strap electrode dampened with water (ground electrode) was placed around the left ankle. The EMG signals were recorded in a monopolar montage, bandpass filtered (10–500 Hz), and digitized at a sampling rate of 2048 Hz using a multichannel acquisition system (EMG-Quattrocento; 400-channel EMG amplifier; OT Biolelettronica, Italy).

2.3.2. Offline EMG decomposition and motor unit tracking

The EMG signals were decomposed using convolutive blind source separation (24, 25), implemented in the MUedit software (26). Prior to automatic decomposition, the channels were visually inspected and those with low signal-to-noise ratio or artifacts were discarded. The remaining EMG signals were extended and whitened. A fast independent component analysis was performed to retrieve the motor unit spike trains mixed within the EMG signals. Specifically, a separation vector was optimized for each motor unit using a fixed-point algorithm to obtain a sparse motor unit pulse train. Firing times were identified from these pulse trains using a peak detection function and a k-mean classification that separated the high peaks (the firing times) from the low peaks (noise). The distance between the high and low peaks was quantified using the silhouette value, and only the pulse trains with a high distance between the high and low peaks (threshold: 0.9) were retained for the subsequent analyses. The resulting spike trains were then edited manually. Manual editing is an iterative process that involves removing detected peaks that result in erroneous firing rates (outliers), and adding missed firing times that are clearly distinguishable from the noise. The motor unit pulse trains are ultimately recalculated with updated separation vectors and accepted by the operator once all the putative firing times are selected. This procedure was performed according to the guidelines described by Del Vecchio et al. (27), and was demonstrated to be highly reliable across operators (28).

The decomposition was performed independently on each electrode grid. Given that the same motor units could be detected across multiple grids covering the same muscle, duplicate units were identified through analysis of their pulse trains. The pulse trains of pairs of motor units were first aligned using a cross-correlation function to account for a potential delay owing to the propagation time of the action potentials along the fibres. Firing times that occurred within 0.5 ms interval were considered as common between motor units; and motor units that

shared more than 30% of their firing times were considered as duplicates (29). When duplicated motor units were identified, only the motor unit with the lowest coefficient of variation of its inter-spike intervals was retained.

For the first experiment, the decomposition procedure described above was performed on each task separately, that is, each trapezoidal reference contraction and each sinusoidal contraction. For the trapezoidal reference contractions, results are reported for the motor units tracked across all four contractions. For the sinusoidal contractions, results are reported for both the untracked and tracked motor units across all three frequency conditions. To track motor units, the separation vectors of the motor unit identified in one contraction were applied to the extended and whitened EMG signals of the other contractions (30). The resulting spike trains were then compared with those obtained after manual editing. A motor unit was tracked if at least 30% of its spikes were shared. This process was applied to each potential pair of contractions. This automatic process was complemented with visual inspection of the 2D spatial distribution of motor unit action potentials across the 256 electrodes to confirm the accuracy of the motor unit tracking. Notably, motor units were not tracked between the reference and sinusoidal contractions due to a large decrease in motor unit yield. However, we verified that outcomes remained consistent even with the smaller sample of tracked units (results not reported here).

2.3.3. Real-time EMG decomposition

To provide online feedback on the motor unit activity in the second experiment, the EMG signals were decomposed in real-time using an open-source software developed and validated by our team (22). First, EMG signals were recorded during a submaximal trapezoid contraction and decomposed offline to identify the motor unit separation vectors and the centroids of the classes ‘spikes’ and ‘noise’ were calculated with a peak detection function and k-mean classification. As the accuracy of the online decomposition can be improved by manually editing the offline decomposition results (21), manual editing was performed prior to the real-time component of the experiment.

For real-time EMG decomposition, motor unit separation vectors were applied to the incoming segments of 125 ms of EMG signals. Peaks closer to the centroid of the ‘spikes’ class than that of the ‘noise’ class were considered as firing times. Besides the 125 ms incompressible delay, the computational time for visual feedback was typically less than 15 ms (21). We calculated the firing rate of individual motor units as the sum of spikes over

eight consecutive windows of 125 ms. This approach introduced a 500 ms delay in estimating the firing rate, but allowed for smoother and more controllable visual feedback than using instantaneous firing rates (21).

2.4. **Data analysis**

2.4.1. Factor analysis

We conducted a factor analysis on the smoothed firing rates of the motor units identified from the GM or VL muscle during the reference contractions (experiment 1) using the "factoran()" function in Matlab (R2023b, Mathworks, USA). First, the binary spike trains were convolved with a 400-ms kernel Hanning window without a phase shift (12). This corresponds to a 2.5 Hz low-pass filter, which retains the information relevant to force production (31, 32). Subsequently, the four 20-s force plateaus were concatenated, and only motor units continuously firing, without any pause between two firings longer than 400 ms, were included in the analysis. Finally, the smoothed firing rates were detrended (33).

Factor analysis allows for factor rotation, which maximizes the overall correlation between the original variables and latent factors, without requiring the latent factors to be orthogonal. We used *promax* rotation, which aims to simplify the structure of the loading matrix by maximizing the weight of one factor, while minimizing the weights of other factors for each variable. To determine the appropriate number of latent factors, we adopted the method proposed by Cheung et al. (34). This approach involves selecting the minimal number of latent factors beyond which additional factors do not significantly improve the model's capability to reconstruct the data over what would be expected from fitting random noise. First, we iterated the factor analysis by varying the number of latent factors between one and ten. For each number of latent factors, the reconstruction accuracy was calculated as the r-squared value between the reconstructed and the original data. We also generated a surrogate dataset through a random permutation of the motor unit spike trains. The surrogate dataset had the same number of spikes and the same mean firing rate as the original dataset. We performed factor analysis on this surrogate dataset, and the r-squared value was calculated for each latent factor from one to ten. The slope of the r-squared curve for the surrogate data was determined by fitting a straight line using least squares regression. The critical number of factors was determined as the maximum count at which the slope of the r-squared curve of the original dataset exceeded that of the surrogate data. Beyond this point, additional factors were considered to capture noise. Notably, we also explored alternative methods for selecting

the number of latent factors. One method involved the selection of the number of factors beyond which the increase in r-squared was lower than 5% (35). Another method involved selecting the number of factors at which the r-squared curve plateaued, as indicated by a mean square error of the linear fit being less than 10^{-3} (36).

We also examined whether factor analysis identified latent factors based on the intrinsic properties of motor units. For each participant, we projected the motor units onto the latent factors, assigning each motor unit a position vector in the factor space. The coordinates of this vector reflected the correlation between the unit's smoothed discharge rates and each factor. Motor units were subsequently clustered based on their dominant factor, identified as the factor with the highest magnitude. This approach allowed us to evaluate whether motor unit clustering was associated with firing rate and/or recruitment threshold.

2.4.2. Dispersion and displacement

We calculated two metrics proposed by Marshall et al. (8) to determine whether the firing rates of motor unit populations deviated from the expected behaviour of motor units exclusively receiving a 1-D common input: motor unit displacement and dispersion (Fig. 2). The firing rates of a population of motor units receiving a 1-D common input should constantly vary along a 1-D monotonic manifold in the same direction as that of the common input. If the firing rate of one motor unit increases, all other firing rates should either increase, remain at zero because of a later recruitment threshold, or plateau at the same value because of rate saturation. The motor unit displacement quantifies the difference in firing rates between two motor units when the firing rates of the two units vary in opposite directions. For this, we first computed the maximum non-negative changes in the firing rates between two timestamps, t and t', for a population of *n* motor units.

$$\Delta r(t,t') = max(r1,t - r1,t', r2,t - r2,t', \ldots, rn,t - rn,t')$$

If all the motor unit firing rates vary in the same direction, then either $\Delta r(t,t')$ or $\Delta r(t',t)$ should be equal to 0. The displacement d(t) was considered as the minimum value between $\Delta r(t,t')$ and $\Delta r(t',t)$. Of note, we quantified the displacement values while iteratively adding time lags τ and τ' of up to 25 ms to t and t', respectively, to account for differences in conduction velocities between motor neurons. Therefore, we maintained the minimal displacement value between $\Delta r(t + \tau, t' + \tau')$ and $\Delta r(t' + \tau', t + \tau)$. Finally, we considered the

displacement for a population of motor units as the maximum value out of all the time stamps t.

Dispersion quantifies the maximal deviation of variations in firing rates from a 1D manifold at the population level. Thus, the summed firing rates of a population of motor units receiving a 1-D common input, equivalent to its L1-norm $\|r\|$, should always be associated with the same population state, that is, the distribution of firing rates within the population. Any change in L1-norm within a population of motor units for a given norm value l would mean that at least two motor units have different firing rates for the same summed firing rate. The dispersion quantifies the maximal difference between L1-norms for a given norm value λ.

$$disp(\lambda) = \max(\|rt1 - rt2\|)$$

We further quantified the dispersion values while iteratively adding time lag vectors τ and τ' of up to 25 ms to the population of the motor units.

Note that we calculated the displacement and dispersion metrics for all possible pairs of motor units. To facilitate the comparison of motor unit flexibility between muscles and motor tasks with different mean firing rates, we normalized the displacement and dispersion values by dividing the values by the sum of the maximum firing rates of the motor units in each pair.

2.4.3. Distance between motor units

To approximate the distance between motor units within the muscle, motor unit action potential waveforms were calculated by spike-trigger-averaging the differential EMG signals over 50 ms windows for each grid of electrodes. The peak-to-peak amplitude of each waveform was calculated, resulting in a 12x5 array of amplitude values for each grid and motor unit. To mitigate the risk of encountering aberrant values due to the presence of artifacts in the EMG signal, we applied a 3x3 box blur kernel to each of the 12x5 arrays. The electrode with the highest amplitude value across the four grids was considered as the approximate location of the motor unit. These positions were then used to calculate the distances between motor units for all possible pairs, assuming an 8 mm inter-electrode distance and a 24 mm inter-grid distance.

2.4.4. Recruitment threshold

Recruitment time was defined as the time of the first firing of a series of three firings occurring within a second. For each motor unit, the recruitment threshold was calculated as the average torque (expressed as a percentage of MVC) recorded at the recruitment times across all contractions.

2.5. Spiking neural network model

We used the Brian2 package implemented in Python (37) to simulate the behaviour of motor neuron populations under seven different scenarios: (i) a single common excitatory input, (ii) three excitatory inputs distributed homogeneously or (iii) heterogeneously, (iv) three inhibitory inputs distributed homogeneously or (v) heterogeneously, (vi) homonymous recurrent inhibition, and (vii) both homonymous and heteronymous recurrent inhibition. The code and the list of parameters are publicly accessible at:
https://github.com/FrancoisDernoncourt/Motor_unit_flexibility

2.5.1. Motor neuron model

We used a conductance-based leaky integrate-and-fire model where each neuron was defined by a resting membrane potential and reset voltage E_{rest} of 0 mV, and a firing threshold V_{thresh} of 10 mV. The voltage change per timestep $\frac{dv}{\mathrm{d}t}$ was calculated based on the leak current I_{leak} (in nA), excitatory current I_{excit} (in nA), inhibitory current I_{inhib} (in nA), and the membrane capacitance C (in F), using the following equation:

$$\frac{dv}{\mathrm{d}t} = \frac{-(I_{leak} + I_{excit} + I_{inhib})}{C}$$

The current values were calculated based on the specific conductance values (g) and equilibrium potential (E), as follows:

$$I_{leak} = g_{leak} \times (v - E_{rest})$$

$$I_{excit} = \max(g_{excit} \times (v - E_{excit}) + I_{rheobase}\ , 0)$$

$$I_{inhib} = g_{inhib} \times (v - E_{inhib})$$

An offset $I_{rheobase}$ was applied to the excitatory current, representing the minimum current required for the excitatory conductance to be non-zero. E_{excit} was set to 25 mV, and E_{inhib} to

-15 mV. These values ensured that excitatory and inhibitory inputs produced voltage changes of equal magnitude when the membrane potential was halfway between E_{rest} and V_{thresh}.

The conductance values (in mS) were defined as:

$$g_{leak} = \frac{1}{R_i}$$

$$g_{excit} = \gamma_{excit}(t,i) \times S_i$$

$$g_{inhib} = \gamma_{inhib}(t,i) \times S_i$$

where R_i (in Ohms) represents the membrane resistance of motor neuron i, $\gamma_{excit}(t,i)$ and $\gamma_{inhib}(t,i)$ are the time-dependent excitatory and inhibitory synaptic inputs delivered to motor neuron i at each timestep t, and S_i is a scaling factor representing the responsiveness of the membrane potential to a given input. S_i values were calculated as the normalized resistance of motor neurons, with S_i of the smallest motor neuron set to 1. After firing, motor neurons underwent a refractory period $T_{refractory}$ during which the membrane potential was clamped to 0 mV.

Each motor pool consisted of 300 simulated motor neurons. Each motor neuron i within a pool was assigned a specific soma diameter D_i (ranging from 50 [D_{min}] to 100 [D_{max}] µm) based on the following quadratic function:

$$D_i = D_{min} + (\frac{i}{N})^2 \times (D_{max} - D_{min})$$

This distribution ensured a higher representation of low-threshold motor neurons (38). The relationship between the soma diameter and R, C, $I_{rheobase}$ and $T_{refractory}$ was determined using the equations provided by Caillet et al. (39) (for further details, please refer to the code).

2.5.2. Input to the simulated motor neurons

The simulated motor neurons received a mixture of inputs in proportions similar to those proposed by Farina & Negro (40): 25% excitatory and/or inhibitory signals (0-2.5 Hz bandwidth), and 75% independent noise (0-50 Hz bandwidth). These input signals had a mean of 0 mS and a standard deviation of 0.03 mS, and they were added to a baseline excitatory input. The baseline excitatory input ranged from 0.5 mS in scenarios with only excitatory inputs (scenarios i, ii, and iii) to 0.78 mS in the scenario involving recurrent

inhibition from homonymous and heteronymous pool (scenario vii). When present, the baseline inhibitory input was set to 0.12 mS.

The common inhibitory inputs and the independent inputs were modelled as low-pass-filtered Gaussian noise with cutoff frequencies of 2.5 and 50 Hz, respectively. The excitatory common inputs were defined as the standardized first principal component(s) derived from the smoothed firing rates recorded during the reference contraction, implying that these excitatory inputs were orthogonal. However, in the scenario involving recurrent inhibition across heteronymous motor pools, we applied an arbitrary pairwise correlation coefficient of approximately 0.7, ensuring that these (synergistic) pools received correlated inputs, consistent with the high proportion of shared inputs observed among the Vastii (19, 41).

When inputs were homogeneously distributed, each motor neuron received an equal proportion of each input. In scenarios with heterogeneous distribution, input weights were randomly sampled from a uniform distribution ranging from 0 to 1 and then processed using a softmax function with a temperature parameter of 0.1. This procedure ensured that the weights summed to one while preserving a heterogeneous distribution of inputs.

2.5.3. Recurrent inhibition simulation

In scenarios vi and vii, we incorporated Renshaw cells into the model as simple integrate-and-fire neurons. The membrane voltage of each Renshaw cell evolved according to:

$$\frac{dv}{\mathrm{d}t} = \frac{I_{Renshaw} - v}{\tau}$$

where $I_{Renshaw}$ is the baseline independent input (in mV), and τ is the time constant set to 8 ms (18, 42). Each Renshaw cell had a resting membrane potential and reset voltage of 0 mV, a firing threshold of 10 mV, and a refractory period of 10 ms.

Each Renshaw cell received independent input modelled as zero-mean, 50 Hz low-pass-filtered Gaussian noise with a standard deviation of 3 mV. The excitatory post-synaptic potential from a motor neuron to its target Renshaw cells was 1.5 mV, and the inhibitory post-synaptic potential from a Renshaw cell to its target motor neurons was 0.002 mS. There was a 5-ms synaptic delay in both directions (from motor neuron to Renshaw cell and from Renshaw cell to motor neuron).

Scenario vi represented homonymous recurrent inhibition with a uniform probability of connectivity between Renshaw cells and motor neurons. Specifically, the model included 60 Renshaw cells serving a single pool of motor neurons. Each Renshaw cell received input from a random subset of 17% of the motor neurons, while each motor neuron received input from approximately 40% of the Renshaw cells. This connectivity pattern was designed to align with previous simulations (42).

Scenario vii included both homonymous and heteronymous recurrent inhibition. We simulated three pools of motor neurons, each associated with a dedicated set of 60 Renshaw cells. Within each pool, each Renshaw cell received input from a random subset of 50% of the homonymous motor neurons, while no input was received from heteronymous motor neurons. Conversely, each motor neuron received input from 60% of the Renshaw cells from its own pool. To include heteronymous connections, each motor neuron pool was divided into three subgroups. One subgroup received additional inhibitory input from 60% of the Renshaw cells of one heteronymous pool, another subgroup received input from 60% of the Renshaw cells of the other heteronymous pool, and the third subgroup received no heteronymous inhibition. Importantly, all motor neurons were consistently inhibited by their homonymous Renshaw cells, and any heteronymous recurrent inhibition originated from a distinct, non-overlapping set of Renshaw cells. This configuration aligns with evidence that recurrent inhibition can be topographically organized across homonymous and synergist pools (43, 44). Of note, when considering all three pools together, the overall percentages of connections between motor neurons and Renshaw cells were similar to those used in scenario vi.

2.5.4. Simulation parameters and analysis of simulated data

Each simulation lasted 60 s. The input amplitudes, as well as the excitatory and inhibitory post-synaptic potentials of motor neurons and Renshaw cells, were manually adjusted to produce physiologically plausible firing rates (8–10.5 Hz for motor neurons and 20–25 Hz for Renshaw cells). We preprocessed and analysed the simulated motor neuron spike trains following the same procedure applied to the experimentally recorded data (see above). In each simulation, approximately 120 to 150 motor neurons out of the 300 were continuously active and were therefore included in the factor analysis. In scenario vii, the factor analysis was performed only on the first motor neuron pool.

2. 5. Statistical analysis

All statistical analyses were conducted using the R software (R Development Core Team, 2023). The significance threshold was set to 0.05 and adjusted using the Bonferroni correction for multiple tests. Logistic regression models were used to compare the *dispersion* and *displacement* values (dependent variables) between the muscles and contraction types (predictors), with one model per dependent variable. In all models, 'Muscle' (GM-GM; VL-VL), 'Contraction type' (sinusoidal 0.25 Hz; sinusoidal 1 Hz; sinusoidal 3 Hz, all sinusoids) and the interaction between 'Muscle' and 'Contraction type' were specified as fixed factors. For each dependent variable, we compared three different model structures with random effects of increasing complexity: no random effects, one intercept per participant, and one intercept per contraction type per participant. Notably, we did not use the 'Muscle' factor in the random effect because the VL and GM experiments involved different participants. In all cases, using one intercept per contraction type per participant as a random effect resulted in the lowest Akaike information criterion and Bayesian information criterion values ($p<0.001$). The selected models thus had the following structure: *"model <= lmer(dependent_variable [dispersion or displacement] ~ muscle * contraction_type + (contraction_type | participant))"*. The statistical significance of the fixed factors were tested using the "anova()" function. Post-hoc pairwise comparisons consisted of contrasting estimated marginal means against each other with Bonferroni-adjusted repeated t-tests. These comparisons were performed using the "emmeans()" function (emmeans package). When testing for the effect of contraction types conditioning on muscles, a repeated-measures design was considered.

To assess whether factor analysis tended to cluster motor units based on their intrinsic properties, we used logistic regression models with motor unit mean firing rates or recruitment thresholds as the dependent variable and the dominant latent factor as the predictor, including participant as a random effect. The model syntax was: *"model <= lmer(dependent_variable [firing_rate or recruitment_threshold] ~ dominant_factor + (dominant_factor | participant))"*. To determine whether the dispersion or displacement scores of motor unit pairs were associated with the distance between the units, we used linear mixed models. The syntax for these models was: *"model <= lmer(dependent_variable [dispersion or displacement] ~ distance + (contraction_type | participant))"*.

3. Results

3.1. Experiment 1: torque-matched contractions

Participants performed either isometric knee extension or plantarflexion tasks. These tasks consisted of matching either a trapezoidal target at 20% MVC (referred to as "reference" contractions), or a sinusoidal target oscillating between 15% and 25% MVC at three different frequencies: 0.25, 1, and 3 Hz (referred to as "sinusoidal" contractions). EMG signals were recorded with grids of surface electrodes A blind source-separation algorithm (24) was applied to the EMG signals to identify motor units spike trains. Using multiple grids of electrodes per muscle optimized the spatial sampling of motor unit surface action potentials (23), resulting in a large sample of identified motor units (VL: up to 60 motor units/participant and GM; up to 67 motor units/participant).

3.1.1. Low-dimensional analysis

We applied a linear dimensionality reduction method, a common approach to characterize the dynamics of populations of neurons (45–48). In our study, dimensionality reduction was applied to the firing rates of the detected motor units to identify a low-dimensional latent space. Specifically, we conducted a factor analysis on the motor units that continuously fired during the plateau phase of the reference contractions (Fig. 1). This analysis included an average of 38.1 ± 8.1 (range: 26-48) motor units per participant for the VL, and 28.0 ± 19.8 (range: 9-60) motor units per participant for the GM. To determine the dimensionality of the latent space, we identified the number of latent factors beyond which adding another factor did not improve the model's ability to reconstruct the data beyond what would be expected from fitting random noise (34). Using this approach, we identified three latent factors in the VL muscle for all participants, accounting for 55% ± 7% (range: 43%-65%) of the total variance in motor unit firing rates. When considering the GM muscle, only one latent factor was identified in five out of six participants, accounting for 69% ± 11% (range: 52%-82%) of the total variance. For the remaining participant, two latent factors were identified, accounting for 60% of the total variance. Notably, we also used alternative methods to determine the number of latent variables (35, 36), which yielded the same results (see the Methods section). These results indicate a distinct dimensionality of the latent spaces of the VL and GM muscles, as suggested by previous work (12, 49). We also examined whether the latent factor representation of VL motor units was influenced by firing rates or recruitment thresholds rather than by the dimensionality of their inputs. No significant association

emerged between dominant factors and either recruitment thresholds (P = 0.323) or mean firing rates (P = 0.17), suggesting that the dimensional structure is not determined by these intrinsic properties.

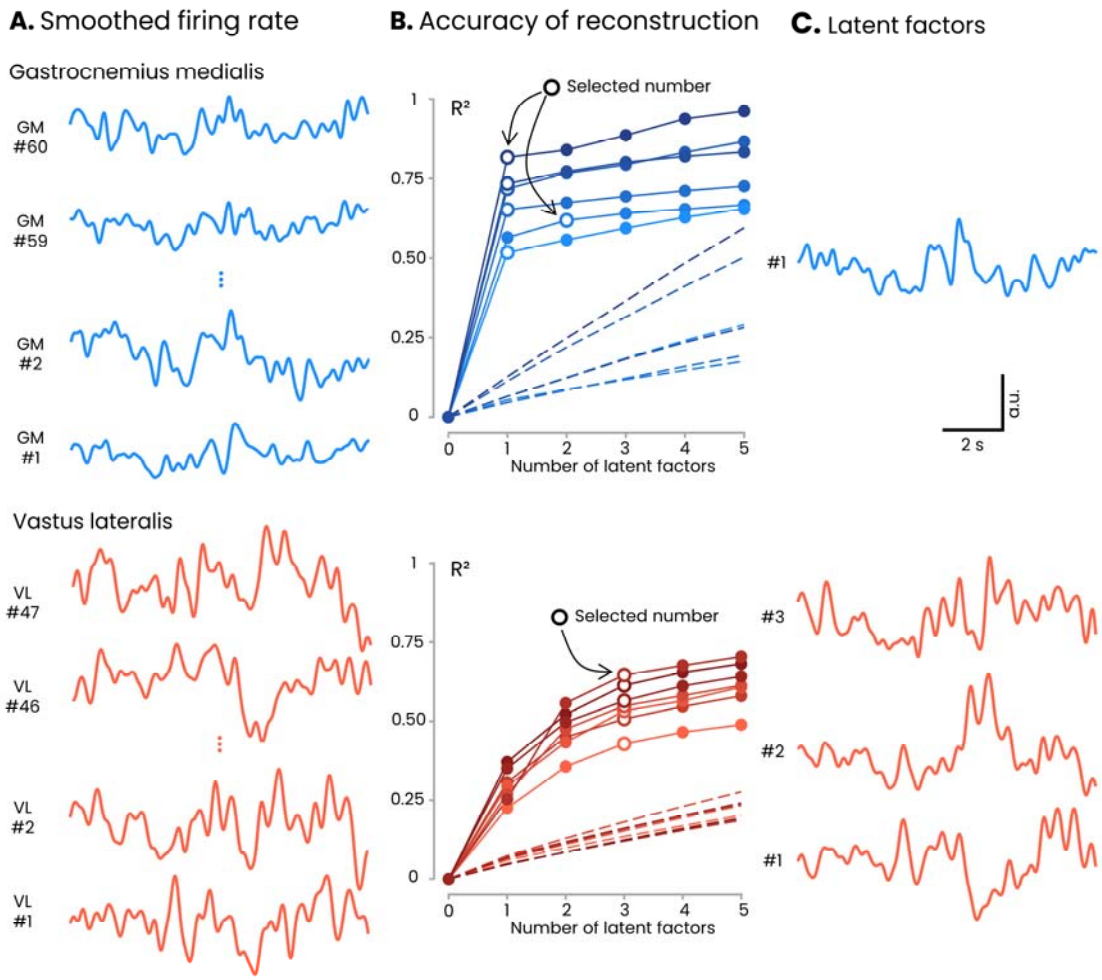

Figure 1 – Dimensionality of motor unit behaviour. (A) Individual example of the smoothed firing rate of motor units identified in the GM (Gastrocnemius medialis, upper panel) and the VL (vastus lateralis, lower panel). In these individual participants, 60 motor units were identified in the GM and 47 in the VL. These smoothed firing rate patterns were used as input to the factor analysis. **(B)** For each number of latent factors (1 to 10, only 5 of which are shown here), we calculated the reconstruction accuracy as the r-squared between the reconstructed and the original data. Each participant is represented by a different shade of blue/red. The dashed lines represent the variance explained for the surrogate data generated by shuffling the inter-spike intervals of the recorded motor units (see Methods). The number of identified latent factors (white-filled dots) corresponds to the point at which the slope of the r-squared curve from experimental data becomes lower than the slope for the surrogate data. **(C)** Latent factors identified for an individual participant. a.u. arbitrary unit.

3.1.2. Flexibility in the motor unit control

Based on recent work reporting flexibility in recruitment during sinusoidal tasks (8), we evaluated the motor unit recruitment during isometric contractions with sinusoidal force profiles at various frequencies. Specifically, flexibility was quantified using two metrics: *dispersion* and *displacement* (8) (Fig. 2). The rationale for using these metrics is based on the premise that the rigid control of motor units by a single common input would constrain the trajectory of their firing rate along a 1-dimensional (1-D) monotonic manifold. While small deviations from this monotonic 1-D manifold would reflect the presence of synaptic noise, large deviations would suggest that the motor units receive distinct inputs, resulting in a certain level of flexibility. These two metrics are formally defined in the Methods section. Across the three contraction frequencies, this analysis included a mean of 39.2 ± 7.6 motor units per participant for the VL (mean number of pairs: 5723 ± 1862), and 27.5 ± 16.9 (mean number of pairs: 3854 ± 3364) motor units per participant for the GM. We also calculated *dispersion* and *displacement* across all three tasks concatenated, using motor units successfully tracked across all three tasks, resulting in 186 GM-GM pairs and 1239 VL-VL pairs.

In this paragraph, "motor unit pairs" (GM-GM and VL-VL) refers to the *Muscle* effect, while the "frequency of the sinusoidal contractions" (0.25, 1, 3 Hz, and all sinusoids) refers to the *Contraction* effect. Although there was no significant main effect of *Muscle* on either *dispersion* ($p=0.34$) or *displacement* ($p=0.99$), we did observe a significant main effect of *Contraction* ($p<0.001$ for both metrics), as well as a significant interaction between *Muscle* and *Contraction* ($p<0.001$ for both metrics). For the sake of clarity, we present only the differences between muscles that are directly relevant to our main objective. There was no difference between the GM and VL neither for *dispersion* nor for *displacement* in all conditions (all $p>0.10$), except for the 1-Hz sinusoidal contraction, during which the GM motor units displayed higher dispersion ($p<0.001$) and higher displacement ($p<0.001$) than the VL motor units (Fig. 2). Further, we noted no significant correlation between the distance separating the two motor units on the skin surface (as evaluated from their action potentials across the four grids) and the degree of flexibility, as measured using *dispersion* (mean r value across participants/conditions: 0.03±0.12, $p=0.20$) or *displacement* ($r=-0.01\pm0.11$, $p=0.42$).

To determine whether the level of flexibility estimated through *dispersion* and *displacement* was significant or negligible, we calculated both metrics for pairs of motor units from the RF

and VL muscles. Given that the RF muscle is biarticular, and can be activated independently of the vastus muscles (50), the *displacement* and *dispersion* values for pairs of RF-VL motor units were used to provide insights into the expected degree of flexibility of motor units that receive different inputs. From a relatively low number of units identified in the RF (5.4±4.6 motor units per participants), we identified a higher flexibility for pairs involving RF compared to the VL-VL or GM-GM pairs (dispersion: +20% and +6% for RF-VL compared to VL-VL and GM-GM across the three conditions, respectively; displacement: +32% and +19% for RF-VL compared to VL-VL and GM-GM across the three conditions, respectively). This suggests that the flexibility observed in both the VL and GM motor units was comparatively small, even though the factor analysis identified three latent factors for the VL.

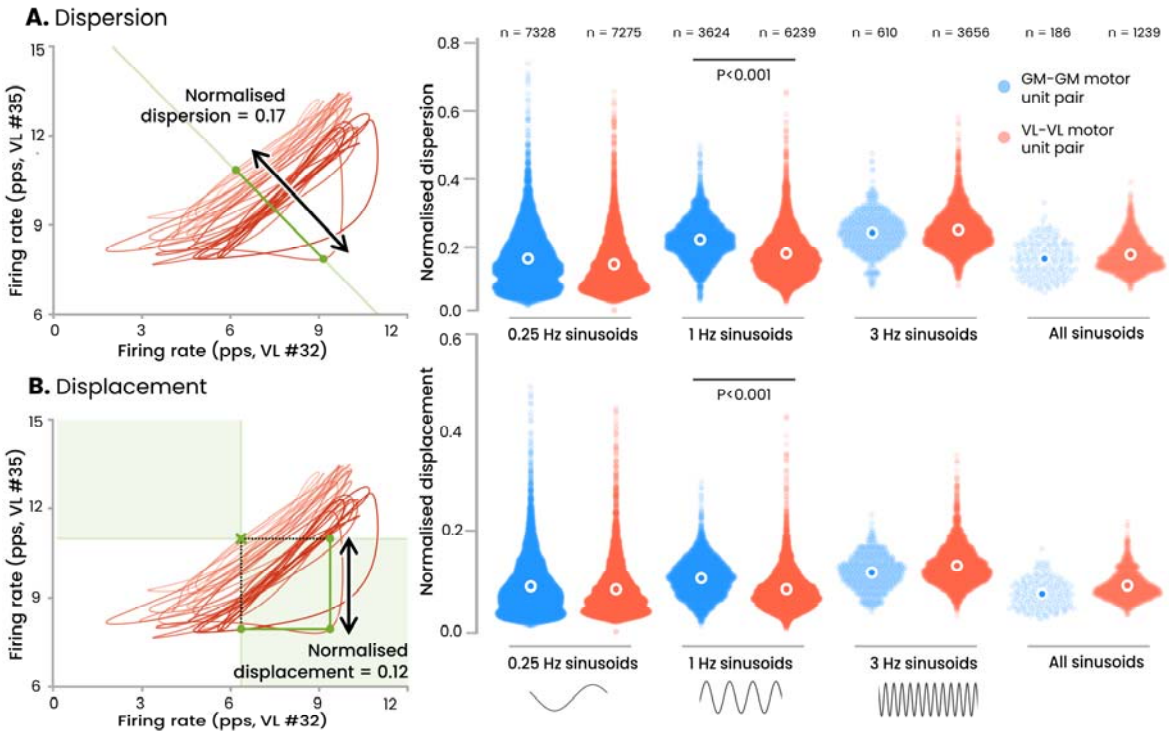

Figure 2 – Motor unit recruitment flexibility during sinusoidal tasks. We evaluated the flexibility in motor unit recruitment during isometric contractions with sinusoidal force profiles at various frequencies (0.25, 1, and 3 Hz) and across all three frequencies combined using motor units matched across conditions ('all sinusoids'). Flexibility was quantified using two metrics: *dispersion* and *displacement* (8). These metrics are based on the premise that the rigid control of motor units would constrain the trajectory of their firing rate along a one-dimensional monotonic manifold (see Methods). The right panels display the normalised values of the dispersion and displacement for each pair of GM-GM and VL-VL motor units, with sample sizes (*n*) indicated above. White circles represent the mean value. There was no difference between muscles, except for the 1 Hz condition, where GM-GM pairs exhibited slightly higher flexibility than VL-VL pairs. GM, gastrocnemius medialis; VL, Vastus lateralis; pps, pulses per second.

3.2. Experiment 2: volitional control of motor units

We performed a second experiment to determine whether the distinct behaviours of the VL and GM motor units reflected a distinct dimensionality of their *volitional* control. Specifically, we assessed whether the participants were able to volitionally dissociate the activity of two motor units from either the GM or the VL when presented with online visual feedback of their firing rates. Visual feedback involved a cursor navigating in a 2-D space, where the cursor coordinates corresponded to the firing rates of the two motor units, each identified in a different muscle region (proximal and distal, see Methods). Two target areas along the x- (Target 1) or y-axes (Target 2) were displayed to the participants (Fig. 3). To position the cursor within these target areas, the participants had to modulate the firing rates of the two motor units independently, that is, increase the firing rate of one unit while maintaining or decreasing the firing rate of the other unit. We tested an average of 2.6±0.5 (VL) and 1.8±0.8 (GM) pairs of motor units per participant (total of 13 pairs for VL and 9 pairs for GM). For each pair of motor units, the participants performed two sets of contractions at either 10% (VL) or 20% MVC (GM). Participants were instructed to reach Target 2 during the first set, and target 1 during the second set. The success rate was calculated as the percentage of time for which the participants maintained the cursor within the targets while producing the required torque (with a margin of +/- 5%) over the total duration of the contraction. For the purposes of analysis, the firing rate of the motor unit with the highest recruitment threshold was depicted on the *y*-coordinate (Target 2). Reaching Target 2 suggests that the participants successfully isolated the activation of the highest threshold unit, demonstrating flexible control. In contrast, reaching Target 1 could be achieved by reducing the neural drive, which could theoretically be compensated by a synergist muscle, and therefore not necessarily indicate flexible control. The success rate associated with Target 1 was 30.4±32.4% for VL and 27.1±23.9% for GM. Interestingly, none of the participants were able to reach Target 2, regardless of the muscle (success rate = 0%).

We further analysed the behaviour of the motor units that were not displayed as feedback to the participants (15.6±7.1 motor units per participant for the VL and 16.6±6.2 motor units per participant for the GM). In very rare cases, we found that Target 2 was reached with these motor units, but with no difference between the two muscles (3.0±12.8% of total time for VL and 3.4±14.0% of total time for GM (p=0.41, t-test). Together, these results support a lack of flexibility in the volitional control of the motor units of the GM or VL muscles, despite the

distinct dimensionality of their manifolds. This conclusion contrasts with the expectation that a greater dimensionality would correspond to a greater number of common inputs of cortical origin (8). Therefore, we analysed other mechanisms that might explain the experimental observation of rigid control with the presence of multiple latent factors in the VL.

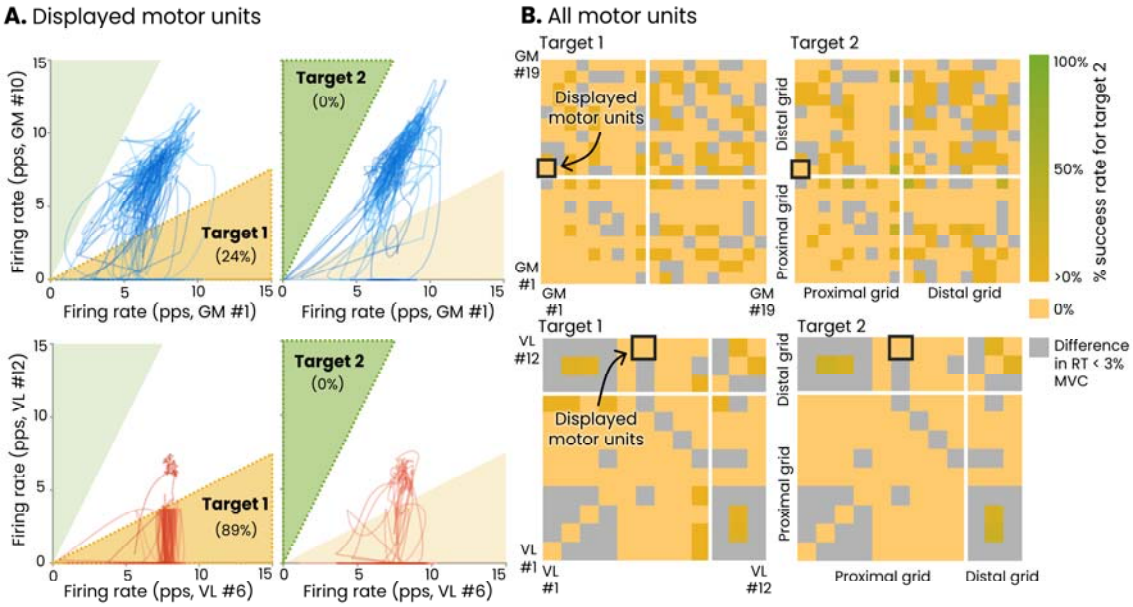

Figure 3 – The online control task with visual feedback. This figure illustrates the results obtained for one representative participant for the gastrocnemius medialis (GM, top panels) and the vastus lateralis (VL, bottom panels). **(A)** The visual feedback involved a cursor navigating in a 2-D space, where the cursor coordinates corresponded to the firing rates of two motor units. Two target areas were displayed: one along the x-axis (Target 1) and one along the y-axis (Target 2). The dark shaded area represents the target the participant was instructed to reach, with the success rate (% of time spent in this target) indicated in parentheses. Note that the firing rate of the motor unit with the highest recruitment threshold is depicted on the *y*-axis (Target 2). Flexible control, defined as deviations from the size principle, is demonstrated by reaching Target 2, which was not achieved by this participant. **(B)** For all the other pairs of motor units identified during this task, but not depicted as feedback, we calculated the success rate as the percentage of time during which the higher threshold motor units had a firing rate twice as high as the lower threshold motor units. This condition is equivalent to reaching Target 2. This analysis was only performed for pairs of motor units with a difference in recruitment threshold > 3% of maximal voluntary contraction (MVC). The pair indicated as 'displayed motor units' are the pairs provided as feedback on Panel A. The vast majority of motor units showed a success rate of 0%. RT, recruitment threshold; pps, pulses per second.

3.3. In-silico models with spiking neural networks

We developed in-silico models to explore the control mechanisms that might explain the differences observed between the GM and VL. Specifically, we tested scenarios of input distribution compatible with the multidimensionality of the linear manifold underlying the behaviour of VL motor units (Fig. 4). The seven scenarios are described in the Methods

section. Factor analysis was applied to the activity of the in-silico motor neurons to estimate the dimensionality of their linear manifolds, following the same approach used for the experimental data.

In the first scenario, which involved a homogeneous distribution of a single common input across motor neurons, only one latent factor was identified, confirming that a pool of motor neurons acts approximately linearly to transmit common inputs (2, 31) (Fig. 4A). Similarly, when three excitatory inputs (scenario ii, Fig. 4B) or three inhibitory inputs (scenario iv, Fig. 4C) were homogeneously distributed across motor neurons, a single latent factor was also identified. Although multiple inputs were present, their uniform distribution made them functionally equivalent to a single common input, albeit with the identified latent factor exhibiting a lower explained variance (r-squared). Scenario vi, which involved homonymous recurrent inhibition, similarly resulted in the identification of a single latent factor, again with a lower explained variance (Fig. 4D). In contrast, when multiple inputs, either excitatory (scenario iii, Fig. 4B) or inhibitory (scenario v, Fig. 4C), were heterogeneously distributed across motor neurons, multiple latent factors were identified. Interestingly, a similar result was observed in scenario vii, which involved a single excitatory input combined with both homonymous and heteronymous recurrent inhibition (Fig. 4E). In that scenario, each motor neuron established excitatory connections exclusively with its homonymous Renshaw cells, and any heteronymous inhibitory input came from a separate, non-overlapping pool of Renshaw cells, thereby producing a multidimensional structure in the motor neuron activity.

It is important to note that the number of factors (three in scenarios iii, v, and vii) was influenced by our chosen parameters, such as the number of input sources and the number of simulated pools. However, the key finding is not the specific number of latent factors but rather that the dimensionality of the motor unit manifold is mainly determined by how the inputs are distributed across the pool. Specifically, when multiple sources of input (excitatory or inhibitory) are distributed uniformly across all motor units, the motor unit activity remains confined within a one-dimensional manifold. In contrast, when these inputs are distributed heterogeneously across motor units, additional dimensions emerged. Together, it demonstrates that it is the non-uniform projection of multiple inputs onto the motor units, rather than the mere presence of multiple inputs (excitatory or inhibitory), that increases the dimensionality of the manifold. Therefore, the differences in dimensionality observed experimentally between VL and GM likely arise from differences in the distribution of inputs and/or the configuration of recurrent inhibitory circuits.

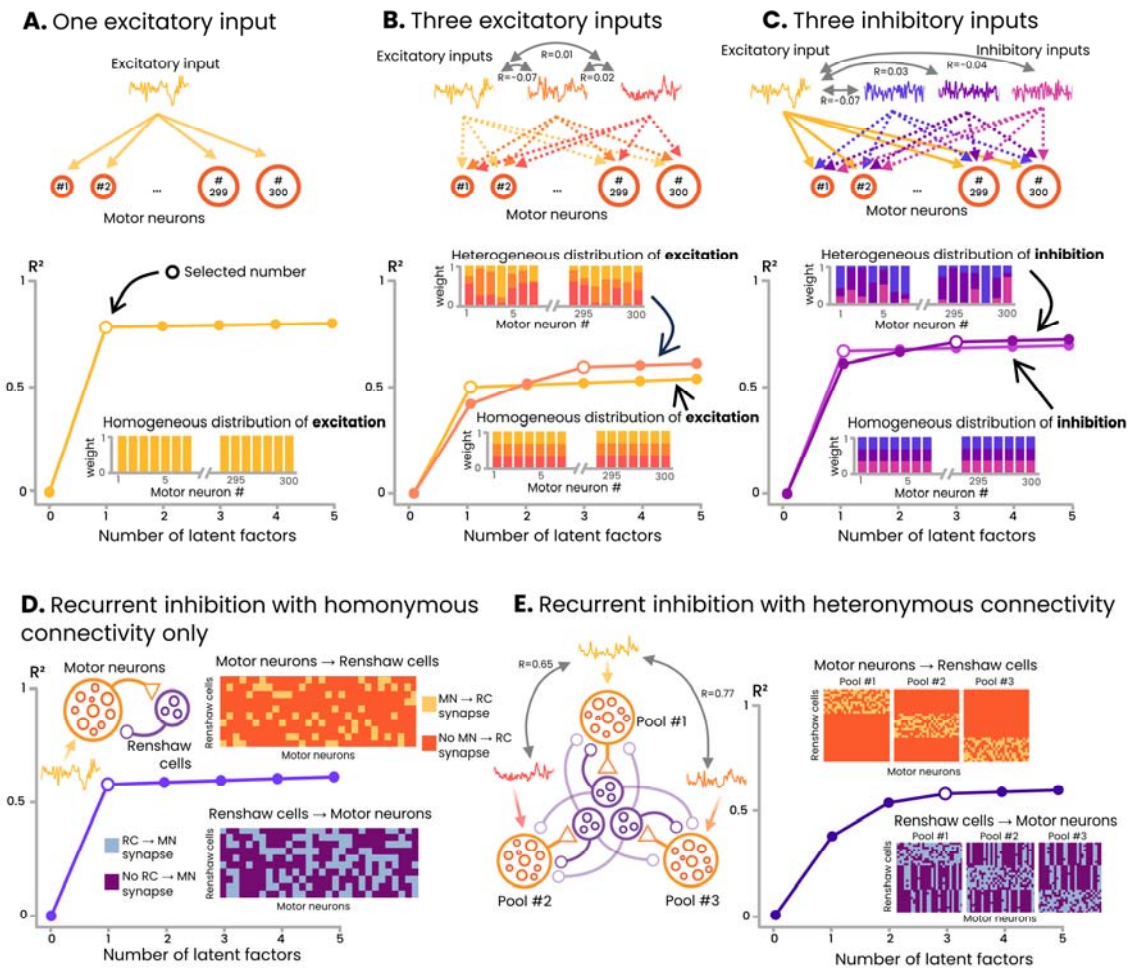

Figure 4 - Simulation scenarios. (A) A single common excitatory input (yellow) was homogenously distributed across 300 motor neurons (bar plot inset), resulting in the identification of one latent factor (scenario i). **(B)** Three uncorrelated excitatory inputs were distributed either homogeneously (scenario ii) or heterogeneously (scenario iii) to the motor neurons. An increase in the number of latent factors was observed only for the heterogeneous distributions. **(C)** Similar to (B), but with three inhibitory inputs in addition to a uniformly distributed common excitatory input. As with excitatory inputs, a homogenous distribution of inhibitory inputs (scenario iv) yielded a single latent factor, whereas heterogeneous distribution resulted in three latent factors (scenario v). **(D)** Recurrent inhibition with random, homonymous connectivity (matrix insets, scenario vi). Providing recurrent inhibition to a single pool of motor neurons via Renshaw cells did not increase dimensionality **(E)** In addition to homonymous connectivity, recurrent inhibition was simulated with heteronymous connectivity between distinct motor neuron pools receiving correlated inputs, potentially representing synergist muscles. Each pool had its own set of Renshaw cells. Importantly, these connections were non-overlapping across heteronymous pools, meaning that each motor neuron provided excitatory inputs exclusively to its own Renshaw cells, and any heteronymous inhibitory input originated from a unique Renshaw cell pool. This arrangement yielded multiple latent factors, demonstrating that non-uniform connectivity patterns can generate multidimensional manifolds despite the presence of a single common excitatory input.

4. Discussion

We investigated the low-dimensional structure of the motor unit activity in two lower limb muscles. By applying a linear dimensionality reduction approach applied to a large sample of motor units, we found that the activity of the GM motor units was effectively captured by a single latent factor defining a unidimensional manifold, whereas the VL motor units were better represented by three latent factors defining a multidimensional manifold. Despite this apparent difference in the manifold dimensionality, the recruitment of motor units in the two muscles exhibited similarly limited flexibility. Using a spiking network model, we demonstrated that the multidimensional manifold formed by the VL motor unit firing activity is compatible with the presence of a single cortical command modulated by either non-homogenously distributed inhibitory inputs or specific configurations of recurrent inhibitory circuits. Taken together, these results suggest that the dimensionality of motor unit linear manifolds is shaped by inputs from both cortical and subcortical sources and does not directly correspond to the dimensionality of volitional control.

There is evidence from anatomically compartmentalized muscles that synchronization between motor units is stronger within muscle compartments than between compartments (51–53). Recent studies have further extended this observation to non-compartmentalized muscles, showing that the behaviour of motor units within the same pool may be more accurately represented by multidimensional linear manifolds (11–14). These results align well with our finding that three latent factors are required to explain the variance in VL motor unit activity. As supported by our simulation (Figure 4B), this could theoretically be explained by the presence of multiple independent supraspinal drives projecting to a single pool (8, 11). However, our experimental observations do not support this hypothesis. Specifically, we found that none of the participants were able to volitionally dissociate the activity of pairs of VL motor units. Furthermore, despite previous studies indicating that tasks with rapid changes in force can trigger flexibility in motor unit recruitment (8, 54), we did not observe any higher flexibility in the VL than in the GM during the fast oscillation tasks. Together, these findings indicate that multidimensionality in motor unit firing manifolds does not necessarily imply the presence of multiple cortical inputs, and is therefore not a sufficient condition for flexible control. Interestingly, although several studies have previously reported multidimensional manifolds of the firings of motor units within (14) and across muscles (55), none have demonstrated clear flexible control in humans under constrained conditions (56). If

the difference in dimensionality in the manifolds for the VL and GM is not due to a different number of cortical inputs, as suggested by the lack of flexibility in control, then a question arises as to how to explain this difference in dimensionality.

Spinal circuits involving muscle or tendon afferents (group Ia, Ib, II, III, and IV) are potential pathways that could contribute to increasing the dimensionality of the motor unit manifold, albeit with limited capacity for volitional control. For example, the distribution of Ia afferents to motor neurons within and between synergist muscles (57) suggests that Ia excitation could introduce additional common excitatory drives. Importantly, our simulation scenarios demonstrate that, regardless of the source of inputs from spinal circuits, these inputs must be distributed non-homogeneously across motor units to increase the dimensionality of the manifold (Figure 4B and C). Of note, a heterogenous distribution of inhibitory inputs has been suggested in response nociceptive stimulation (58, 59). In addition, there is evidence of a regionalization of the stretch reflex in the Vastus medialis muscle, where the activation of Ia afferents from a specific muscle region preferentially activates motor units within the same region (60). However, in our study, we found no significant correlation between the distance separating two motor units on the skin surface and the degree of flexibility, which seems to rule out the involvement of this mechanism in our results. Of note, we are not aware of studies supporting differences in the organization of spinal circuits involving muscle or tendon afferents between the VL and GM muscles. Nonetheless, we cannot definitively exclude the potential contribution of these circuits to our findings.

Among the various neural pathways involved in the control of motor units, recurrent inhibition by Renshaw cells may play a crucial role in the behaviour observed in VL motor units. The role of Renshaw cells in decorrelating the activity of motor units within a pool has been previously discussed (16, 18, 42, 61). Our simulation results indicate that the dynamics of the VL motor units is compatible with specific configurations of recurrent inhibitory circuits involving heteronymous connectivity, even with a single descending command. Specifically, our simulation aligned with the experimental data only when the model incorporated both homonymous and heteronymous recurrent inhibition (Figure 4E). This was in the form of distinct inhibitory inputs driven by synergist muscles, which in our case were putatively the vastus medialis and vastus intermedius muscles. This finding is consistent with previous observations showing that Renshaw cells can be activated by recurrent collaterals of

synergist motor neurons (17, 61, 62). Importantly, the fact that homonymous recurrent inhibition alone did not increase the manifold dimensionality (Figure 4D) suggests that it is not the amount of recurrent inhibition that shapes the manifold, but rather the connectivity of the recurrent inhibitory circuits in the spinal cord. Although we cannot exclude the possibility that the multidimensionality of the VL motor unit activity is an epiphenomenon arising from the complex circuitry of motor pathways serving no functional role, it seems improbable that biological systems would evolve sub-optimal muscle control schemes. Therefore, we argue that the distinct control schemes of the GM and VL are designed to comply with specific functional roles.

Considering the proposed role of recurrent inhibition in limiting the synchrony of motor unit firings (18, 42), heteronymous projections between motor pools likely serve to desynchronise the firings of motor units from different muscles. This may be particularly important for muscles that share a high level of common drive, as is the case between the VL and vastus medialis (19, 41). In such muscle groups, controlling the timing of motor unit discharges to facilitate smooth force production would require both homonymous and heteronymous recurrent inhibitory circuits. In contrast, for muscles that share minimal common drive, such as the GM and its synergists (20, 49), heteronymous circuits would be unnecessary. Together, it supports the functional role of heteronymous recurrent inhibition and the idea that it is large for motor nuclei with consistent activity patterns, whereas it is absent or moderate for motor nuclei that are activated independently (63).

Three key methodological considerations must be addressed. First, our results were obtained at low contraction intensities (up to 20% MVC), primarily reflecting the behaviour of the lowest-threshold motor units. Since our approach required relatively long contractions, higher intensities would likely have induced fatigue, thereby introducing a confounding factor. Of note, investigating higher contraction intensities, where recurrent inhibition is expected to be lower (64), could help elucidate the role of recurrent inhibitory circuits in shaping the dimensionality of the motor unit manifold. Second, we acknowledge that multiple neural pathways could contribute to the observed between-muscle differences in manifold dimensionality. Although we used a spiking neural network model to explore possible scenarios, we cannot draw definitive conclusions about the specific neural circuits responsible for shaping this dimensionality. Third, a previous study involving a rhesus

macaque performing isometric force-tracking tasks reported greater flexibility in motor unit recruitment with chirp force patterns compared to sinusoidal patterns (8). In that study, the monkey was highly trained and capable of accurately tracking complex force patterns. In contrast, our human participants encountered significant challenges in following a 3 Hz sinusoidal force pattern. Introducing a chirp pattern would likely have further increased the difficulty of the task. For this reason, we opted to use a sinusoidal force profile at a constant frequency, balancing the need for dynamic force modulation with the participants' ability to perform the task accurately. Importantly, our conclusion regarding the lack of flexibility is not based solely on the sinusoidal tasks but is primarily supported by the online motor unit control tasks, where participants were free to explore any inputs to the motor units. This approach provided a more direct means for participants to demonstrate volitional, independent control; however, this was not observed. It is important to emphasize that these potential limitations do not undermine our primary conclusion that the multidimensionality of motor unit linear manifolds does not necessarily imply flexible control.

This study demonstrates that the activity of GM motor units can be effectively captured by a single latent factor defining a unidimensional manifold, whereas VL motor units are better represented by three latent factors defining a multidimensional manifold. Despite this difference in dimensionality, the recruitment of motor units exhibited similarly limited levels of flexibility. Our simulations revealed that a heterogeneous distribution of inputs to motor units, or specific configurations of spinal circuits, such as recurrent inhibition, could produce a multidimensional manifold, even with a single descending command. In conclusion, this study highlights that while motor unit firings can lie within a multidimensional manifold, the central nervous system may still lack the capacity for flexible volitional control over these motor units. By extension, these findings suggest that the dimensionality of the linear manifold may not directly reflect descending inputs but could instead be modulated by local spinal circuits.

5. References

1. C. J. de Luca, R. S. LeFever, M. P. McCue, A. P. Xenakis, Control scheme governing concurrently active human motor units during voluntary contractions. *The Journal of Physiology* **329**, 129–142 (1982).

2. F. Negro, A. Holobar, D. Farina, Fluctuations in isometric muscle force can be described by one linear projection of low-frequency components of motor unit discharge rates. *The Journal of Physiology* **587**, 5925–5938 (2009).

3. A. Schmied, J. P. Vedel, S. Pagni, Human spinal lateralization assessed from motoneurone synchronization: dependence on handedness and motor unit type. *The Journal of Physiology* **480**, 369–387 (1994).

4. E. Henneman, Relation between Size of Neurons and Their Susceptibility to Discharge. *Science* **126**, 1345–1347 (1957).

5. J. E. Desmedt, E. Godaux, Spinal motoneuron recruitment in man: rank deordering with direction but not with speed of voluntary movement. *Science* **214**, 933–936 (1981).

6. B. M. Ter Haar Romeny, J. J. D. Van Der Gon, C. C. A. M. Gielen, Changes in recruitment order of motor units in the human biceps muscle. *Experimental Neurology* **78**, 360–368 (1982).

7. U. Herrmann, M. Flanders, Directional Tuning of Single Motor Units. *J. Neurosci.* **18**, 8402–8416 (1998).

8. N. J. Marshall, *et al.*, Flexible neural control of motor units. *Nat Neurosci* (2022). https://doi.org/10.1038/s41593-022-01165-8.

9. E. Formento, P. Botros, J. M. Carmena, Skilled independent control of individual motor units via a non-invasive neuromuscular–machine interface. *J. Neural Eng.* **18**, 066019 (2021).

10. P. N. S. Bawa, K. E. Jones, R. B. Stein, Assessment of size ordered recruitment. *Front. Hum. Neurosci.* **8** (2014).

11. F. Hug, S. Avrillon, J. Ibáñez, D. Farina, Common synaptic input, synergies and size principle: Control of spinal motor neurons for movement generation. *The Journal of Physiology* **601**, 11–20 (2023).

12. A. Del Vecchio, *et al.*, The Forces Generated by Agonist Muscles during Isometric Contractions Arise from Motor Unit Synergies. *J. Neurosci.* **43**, 2860–2873 (2023).

13. S. Madarshahian, M. L. Latash, Synergies at the level of motor units in single-finger and multi-finger tasks. *Exp Brain Res* **239**, 2905–2923 (2021).

14. J. M. Ricotta, *et al.*, Motor unit-based synergies in a non-compartmentalized muscle. *Exp Brain Res* **241**, 1367–1379 (2023).

15. M. Bräcklein, *et al.*, The control and training of single motor units in isometric tasks are constrained by a common input signal. *eLife* **11**, e72871 (2022).

16. D. Adam, U. Windhorst, G. F. Inbar, The effects of recurrent inhibition on the cross-correlated firing patterns of motoneurones (and their relation to signal transmission in the spinal cord-muscle channel). *Biol. Cybernetics* **29**, 229–235 (1978).

17. J. C. Eccles, R. M. Eccles, A. Iggo, M. Ito, Distribution of recurrent inhibition among motoneurones. *The Journal of Physiology* **159**, 479–499 (1961).

18. M. G. Maltenfort, C. J. Heckman, W. Z. Rymer, Decorrelating Actions of Renshaw Interneurons on the Firing of Spinal Motoneurons Within a Motor Nucleus: A Simulation Study. *Journal of Neurophysiology* **80**, 309–323 (1998).

19. S. Avrillon, *et al.*, Individual differences in the neural strategies to control the lateral and medial head of the quadriceps during a mechanically constrained task. *Journal of Applied Physiology* **130**, 269–281 (2021).

20. F. Hug, A. Del Vecchio, S. Avrillon, D. Farina, K. Tucker, Muscles from the same muscle group do not necessarily share common drive: evidence from the human triceps surae. *Journal of Applied Physiology* **130**, 342–354 (2021).

21. J. Rossato, S. Avrillon, K. Tucker, D. Farina, F. Hug, The Volitional Control of Individual Motor Units Is Constrained within Low-Dimensional Neural Manifolds by Common Inputs. *J. Neurosci.* **44** (2024).

22. J. Rossato, *et al.*, I-Spin live: An open-source software based on blind-source separation for real-time decoding of motor unit activity in humans. *eLife* **12** (2024).

23. A. H. Caillet, *et al.*, Larger and Denser: An Optimal Design for Surface Grids of EMG Electrodes to Identify Greater and More Representative Samples of Motor Units. *eNeuro* **10** (2023).

24. A. Holobar, D. Zazula, Multichannel Blind Source Separation Using Convolution Kernel Compensation. *IEEE Transactions on Signal Processing* **55**, 4487–4496 (2007).

25. F. Negro, S. Muceli, A. M. Castronovo, A. Holobar, D. Farina, Multi-channel intramuscular and surface EMG decomposition by convolutive blind source separation. *J. Neural Eng.* **13**, 026027 (2016).

26. S. Avrillon, F. Hug, S. N. Baker, C. Gibbs, D. Farina, Tutorial on MUedit: An open-source software for identifying and analysing the discharge timing of motor units from electromyographic signals. *Journal of Electromyography and Kinesiology* **77**, 102886 (2024).

27. A. Del Vecchio, *et al.*, Tutorial: Analysis of motor unit discharge characteristics from high-density surface EMG signals. *Journal of Electromyography and Kinesiology* **53**, 102426 (2020).

28. F. Hug, *et al.*, Analysis of motor unit spike trains estimated from high-density surface electromyography is highly reliable across operators. *Journal of Electromyography and Kinesiology* **58**, 102548 (2021).

29. A. Holobar, M. A. Minetto, A. Botter, F. Negro, D. Farina, Experimental Analysis of Accuracy in the Identification of Motor Unit Spike Trains From High-Density Surface EMG. *IEEE Trans. Neural Syst. Rehabil. Eng.* **18**, 221–229 (2010).

30. A. Frančič, A. Holobar, "On the Reuse of Motor Unit Filters in High Density Surface Electromyograms with Different Signal-to-Noise Ratios" in *8th European Medical and Biological Engineering Conference*, IFMBE Proceedings., T. Jarm, A. Cvetkoska, S. Mahnič-Kalamiza, D. Miklavcic, Eds. (Springer International Publishing, 2021), pp. 923–931.

31. D. Farina, F. Negro, J. L. Dideriksen, The effective neural drive to muscles is the common synaptic input to motor neurons. *J Physiol* **592**, 3427–3441 (2014).

32. F. Negro, U. Ş. Yavuz, D. Farina, The human motor neuron pools receive a dominant slow-varying common synaptic input. *The Journal of Physiology* **594**, 5491–5505 (2016).

33. C. J. De Luca, Z. Erim, Common Drive in Motor Units of a Synergistic Muscle Pair. *Journal of Neurophysiology* **87**, 2200–2204 (2002).

34. V. C. K. Cheung, *et al.*, Stability of muscle synergies for voluntary actions after cortical stroke in humans. *Proceedings of the National Academy of Sciences* **106**, 19563–19568 (2009).

35. D. J. Clark, L. H. Ting, F. E. Zajac, R. R. Neptune, S. A. Kautz, Merging of Healthy Motor Modules Predicts Reduced Locomotor Performance and Muscle Coordination Complexity Post-Stroke. *Journal of Neurophysiology* **103**, 844–857 (2010).

36. V. C. K. Cheung, A. d'Avella, M. C. Tresch, E. Bizzi, Central and Sensory Contributions to the Activation and Organization of Muscle Synergies during Natural Motor Behaviors. *J. Neurosci.* **25**, 6419–6434 (2005).

37. M. Stimberg, R. Brette, D. F. Goodman, Brian 2, an intuitive and efficient neural simulator. *eLife* **8**, e47314 (2019).

38. J. Duchateau, R. M. Enoka, Distribution of motor unit properties across human muscles. *Journal of Applied Physiology* **132**, 1–13 (2022).

39. A. H. Caillet, A. T. Phillips, D. Farina, L. Modenese, Mathematical relationships between spinal motoneuron properties. *eLife* **11**, e76489 (2022).

40. D. Farina, F. Negro, Common Synaptic Input to Motor Neurons, Motor Unit Synchronization, and Force Control. *Exercise and Sport Sciences Reviews* **43**, 23–33 (2015).

41. C. M. Laine, E. Martinez-Valdes, D. Falla, F. Mayer, D. Farina, Motor Neuron Pools of Synergistic Thigh Muscles Share Most of Their Synaptic Input. *Journal of Neuroscience* **35**, 12207–12216 (2015).

42. E. R. Williams, S. N. Baker, Renshaw Cell Recurrent Inhibition Improves Physiological Tremor by Reducing Corticomuscular Coupling at 10 Hz. *J. Neurosci.* **29**, 6616–6624 (2009).

43. R. M. Brownstone, T. V. Bui, "Spinal interneurons providing input to the final common path during locomotion" in *Progress in Brain Research*, (Elsevier, 2010), pp. 81–95.

44. M. L. McCurdy, T. M. Hamm, Topography of recurrent inhibitory postsynaptic potentials between individual motoneurons in the cat. *Journal of Neurophysiology* **72**, 214–226 (1994).

45. J. P. Cunningham, B. M. Yu, Dimensionality reduction for large-scale neural recordings. *Nat Neurosci* **17**, 1500–1509 (2014).

46. B. DePasquale, D. Sussillo, L. F. Abbott, M. M. Churchland, The centrality of population-level factors to network computation is demonstrated by a versatile approach for training spiking networks. *Neuron* **111**, 631-649.e10 (2023).

47. J. A. Gallego, M. G. Perich, L. E. Miller, S. A. Solla, Neural Manifolds for the Control of Movement. *Neuron* **94**, 978–984 (2017).

48. K. V. Shenoy, M. Sahani, M. M. Churchland, Cortical Control of Arm Movements: A Dynamical Systems Perspective. *Annu. Rev. Neurosci.* **36**, 337–359 (2013).

49. J. Levine, S. Avrillon, D. Farina, F. Hug, J. L. Pons, Two motor neuron synergies, invariant across ankle joint angles, activate the triceps surae during plantarflexion. *The Journal of Physiology* JP284503 (2023). https://doi.org/10.1113/JP284503.

50. F. Hug, P. W. Hodges, K. Tucker, Task dependency of motor adaptations to an acute noxious stimulation. *Journal of Neurophysiology* **111**, 2298–2306 (2014).

51. D. A. Keen, A. J. Fuglevand, Distribution of Motor Unit Force in Human Extensor Digitorum Assessed By Spike-Triggered Averaging and Intraneural Microstimulation. *Journal of Neurophysiology* **91**, 2515–2523 (2004).

52. T. L. McIsaac, A. J. Fuglevand, Motor-Unit Synchrony Within and Across Compartments of the Human Flexor Digitorum Superficialis. *Journal of Neurophysiology* **97**, 550–556 (2007).

53. K. T. Reilly, M. A. Nordstrom, M. H. Schieber, Short-Term Synchronization Between Motor Units in Different Functional Subdivisions of the Human Flexor Digitorum Profundus Muscle. *Journal of Neurophysiology* **92**, 734–742 (2004).

54. L. Grimby, J. Hannerz, Firing rate and recruitment order of toe extensor motor units in different modes of voluntary conraction. *The Journal of Physiology* **264**, 865–879 (1977).

55. J. Rossato, S. Avrillon, K. Tucker, D. Farina, F. Hug, The volitional control of individual motor units is constrained within low-dimensional neural manifolds by common inputs. *J. Neurosci.* e0702242024 (2024). https://doi.org/10.1523/JNEUROSCI.0702-24.2024.

56. C. J. Heckman, R. M. Enoka, “Motor Unit” in *Comprehensive Physiology*, 1st Ed., R. Terjung, Ed. (Wiley, 2012), pp. 2629–2682.

57. F. Baldissera, H. Hultborn, M. Illert, “Integration in Spinal Neuronal Systems” in *Comprehensive Physiology*, 1st Ed., R. Terjung, Ed. (Wiley, 1981), pp. 509–595.

58. F. Hug, *et al.*, Heterogeneous distribution of inhibitory inputs among motor units as a key mechanism for motor adaptations to pain. [Preprint] (2024). Available at: https://www.biorxiv.org/content/10.1101/2024.10.05.616762v1 [Accessed 2 January 2025].

59. P. W. Hodges, *et al.*, Non-uniform Effects of Nociceptive Stimulation to Motoneurones during Experimental Muscle Pain. *Neuroscience* **463**, 45–56 (2021).

60. A. Gallina, J. Blouin, T. D. Ivanova, S. J. Garland, Regionalization of the stretch reflex in the human vastus medialis. *J Physiol* **595**, 4991–5001 (2017).

61. S. A. Edgley, E. R. Williams, S. N. Baker, Spatial and Temporal Arrangement of Recurrent Inhibition in the Primate Upper Limb. *J. Neurosci.* **41**, 1443–1454 (2021).

62. R. Katz, E. Pierrot-Deseilligny, Recurrent inhibition in humans. *Progress in Neurobiology* **57**, 325–355 (1999).

63. T. V. Trank, V. V. Turkin, T. M. Hamm, Organization of recurrent inhibition and facilitation in motoneuron pools innervating dorsiflexors of the cat hindlimb. *Experimental Brain Research* **125**, 344–352 (1999).

64. H. Hultborn, E. Pierrot-Deseilligny, Changes in recurrent inhibition during voluntary soleus contractions in man studied by an H-reflex technique. *J Physiol* **297**, 229–251 (1979).

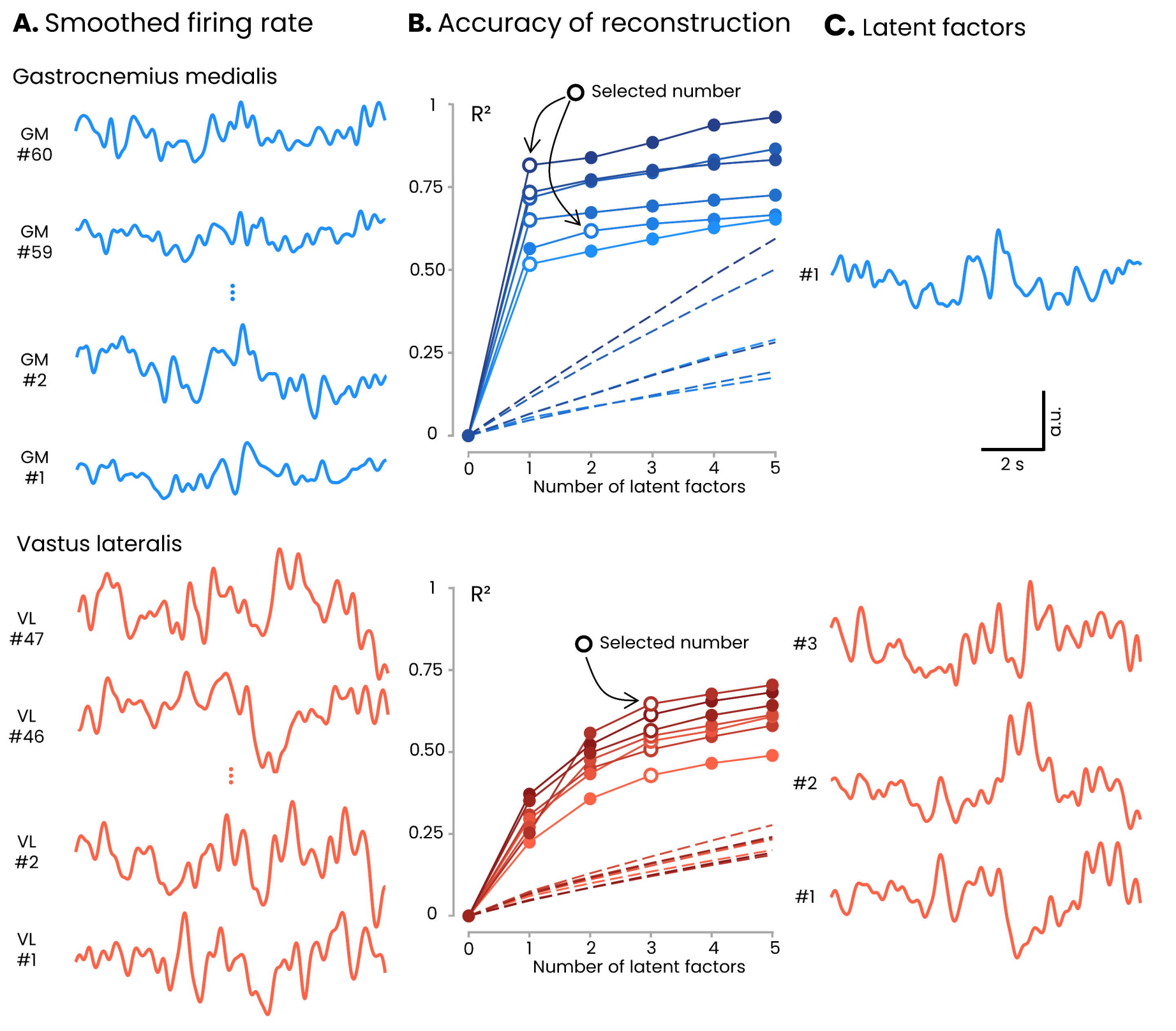
A. Smoothed firing rate
B. Accuracy of reconstruction
C. Latent factors
Gastrocnemius medialis
GM #60
GM #59
GM #2
GM #1
Selected number
R²
1
0.75
0.50
0.25
0
0
1
2
3
4
5
Number of latent factors
#1
a.u.
2 s
Vastus lateralis
VL #47
VL #46
VL #2
VL #1
Selected number
R²
1
0.75
0.50
0.25
0
0
1
2
3
4
5
Number of latent factors
#3
#2
#1

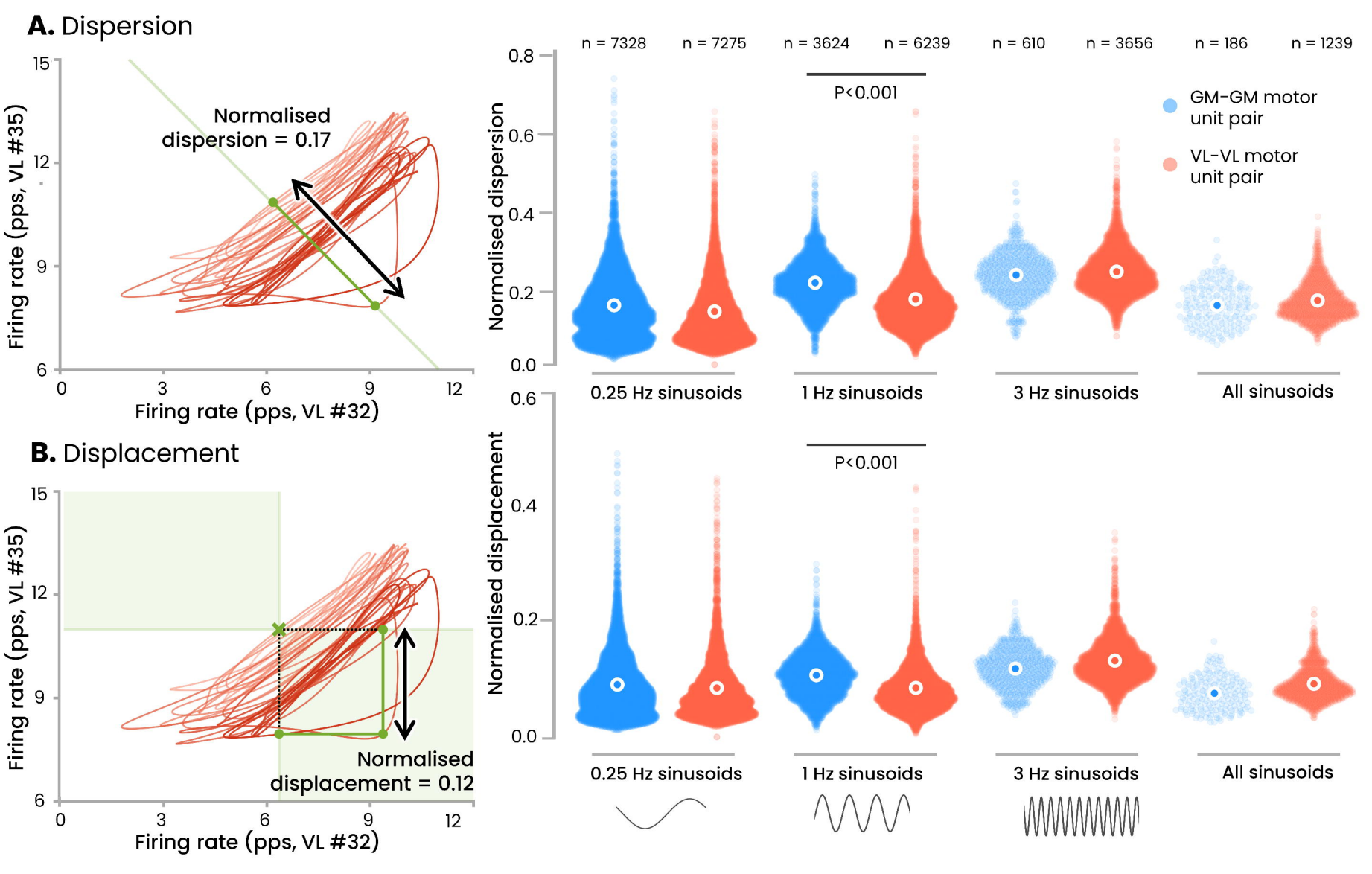
A. Dispersion
Normalised dispersion = 0.17
Firing rate (pps, VL #35)
Firing rate (pps, VL #32)
n = 7328
n = 7275
n = 3624
n = 6239
n = 610
n = 3656
n = 186
n = 1239
P<0.001
GM-GM motor unit pair
VL-VL motor unit pair
Normalised dispersion
0.25 Hz sinusoids
1 Hz sinusoids
3 Hz sinusoids
All sinusoids
B. Displacement
Normalised displacement = 0.12
Normalised displacement

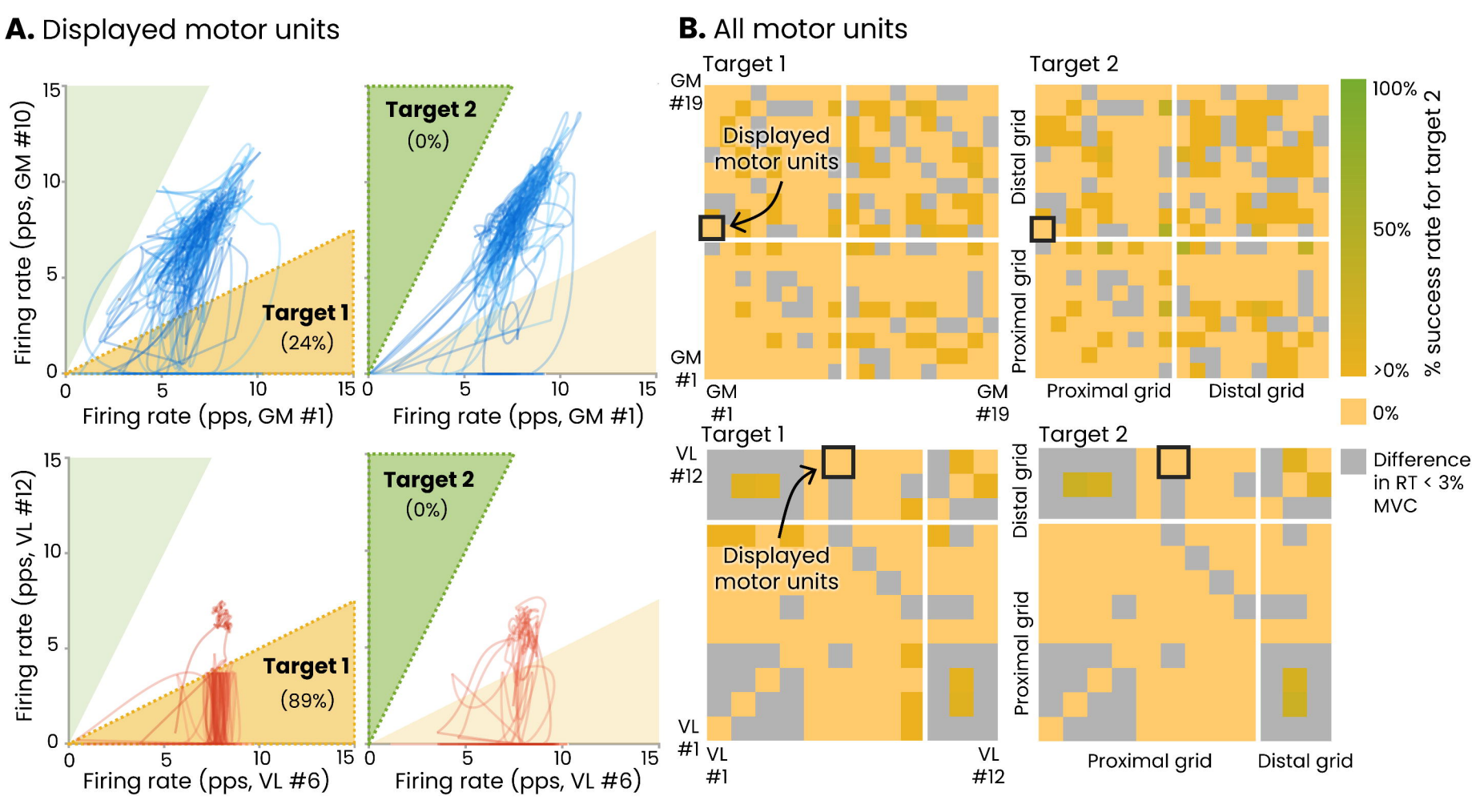
A. Displayed motor units
B. All motor units
Target 1
(24%)
Target 2
(0%)
Target 1
(89%)
Target 2
(0%)
Firing rate (pps, GM #10)
Firing rate (pps, GM #1)
Firing rate (pps, VL #12)
Firing rate (pps, VL #6)
Target 1
Target 2
Displayed motor units
GM #19
GM #1
VL #12
VL #1
Distal grid
Proximal grid
100%
50%
>0%
% success rate for target 2
0%
Difference in RT < 3% MVC

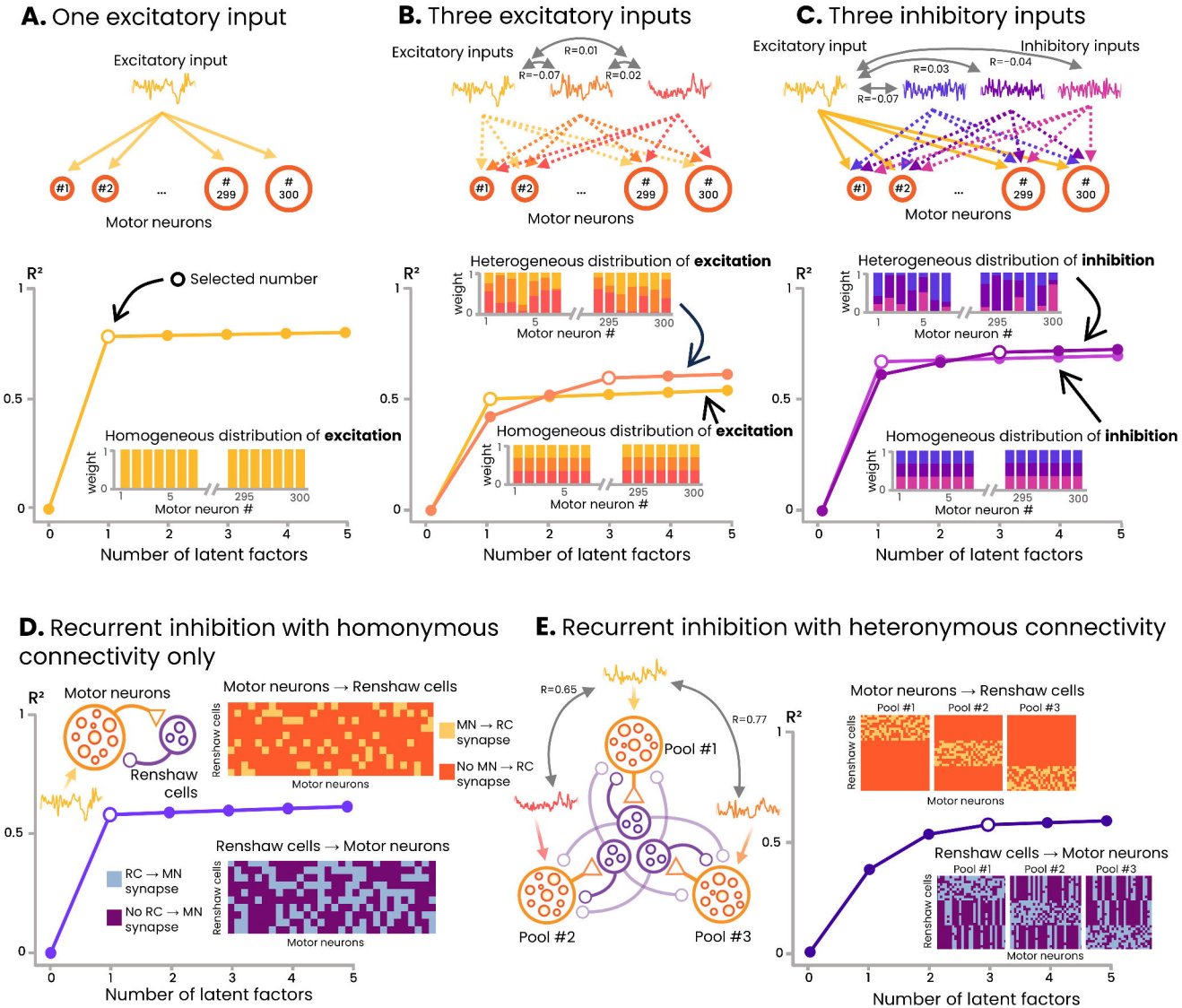
A. One excitatory input
Excitatory input
#1
#2
...
299
300
Motor neurons
R²
Selected number
Homogeneous distribution of excitation
weight
Motor neuron #
Number of latent factors
B. Three excitatory inputs
Excitatory inputs
R=0.01
R=-0.07
R=0.02
Heterogeneous distribution of excitation
Homogeneous distribution of excitation
C. Three inhibitory inputs
Excitatory input
Inhibitory inputs
R=0.03
R=-0.04
R=-0.07
Heterogeneous distribution of inhibition
Homogeneous distribution of inhibition
D. Recurrent inhibition with homonymous connectivity only
Motor neurons
Renshaw cells
Motor neurons → Renshaw cells
MN → RC synapse
No MN → RC synapse
Renshaw cells → Motor neurons
RC → MN synapse
No RC → MN synapse
E. Recurrent inhibition with heteronymous connectivity
R=0.65
R=0.77
Pool #1
Pool #2
Pool #3
Motor neurons → Renshaw cells
Renshaw cells → Motor neurons